*Progress In Electromagnetics Research M, Vol. 103, 27–36, 2021*

# Eigenbeam Analysis of Singly Curved Conformal Antenna Array

**Irfanullah[1, *], Hina Munsif[1], and Ali I. Najam[2]**

**Abstract**—In this paper, eigen analysis of the correlation matrix for an 8-element singly curved conformal antenna array with plane wave(s) incident at different angles is presented. The signal eigenvectors derived from the correlation matrix are used as the array weights to generate peak beams toward the directions of the signals, and the noise eigenvectors derived from the correlation matrix are used as the array weights to generate nulls in the directions of the signals. A $1 \times 8$ microstrip patch antenna array is embedded on an anhedral corner type structure with different amount of surface deformation to analyse the array pattern. The patch antenna elements in the conformal array are excited with attenuators (for amplitude control) and phase shifters (for phase control) to implement the complex signal eigenvectors practically. The simulated eigenbeams using conformal antenna array are in good agreement with the measurement results. Furthermore, the effects of surface deformation on gain and beamwidth of array main beam is discussed. The proposed eigenbeam conformal antenna array can be used in smart and adaptive array applications.

## 1. INTRODUCTION

Recently, industrial and academic research on conformal antennas is rising due to their flexibility of placing antenna elements on non-planar surfaces [1]. A lot of research materials are available on beamforming using linear and planar antenna arrays to generate the desired radiation patterns [2, 3]. However, in the open literature, very few research articles are available on beamforming using conformal surfaces due to the complexity of surface geometries and contributions of surface dependent individual antenna element patterns in the overall array pattern. Beamforming using conformal surfaces is required in various engineering applications, for example in body area networks [4–6], for wireless communication applications [7, 8], and for aerial platforms [9, 10]. Here, the most relevant literature review on beamforming using singly curved conformal surfaces is presented. In [11], 16 patch antenna elements are placed on a corner reflector (singly curved conformal surface) to study the effects of static and dynamic deformed array radiation patterns. Computations of weights for deformed phased array are done using physical optics (PO) approximation. The PO method can be applied to smaller angles of surface deformations. The eigen-correlation method in the proposed work is applicable to both small and large angles of surface deformations. In [12], a 4-element printed monopole linear antenna array is embedded in small unmanned aerial vehicle (UAV) wing structures for beam steering, where the wings are assumed to be flat. The algorithm has not been demonstrated for flexing wing structures, as it works only for a flat antenna array in the wing structure. In [13], a $1 \times 4$ flexible antenna array system for deformable wing surfaces is presented to correct the orientation of broadside main beam by applying the compensated phase difference between the antenna elements. In [14–16], wedge-shaped (singly curved) and cylindrical-shaped conformal antenna arrays are investigated to recover the broadside distorted radiation patterns without main beam scanning. In [17–21], beamforming using a conformal antenna array (other than singly curved) is presented with no or very little open information

*Received 12 May 2021, Accepted 8 June 2021, Scheduled 15 June 2021*
* Corresponding author: Irfanullah (eengr@cuiatd.edu.pk).
[1] Department of Electrical & Computer Engineering, COMSATS University Islamabad, Abbottabad Campus, Abbottabad, Pakistan.
[2] National Electronics Complex of Pakistan (NECOP), Islamabad, Pakistan.

available on calculating the beamforming weights. The above mentioned study suggests that designing a beamforming conformal array with a simple technique and open information applicable to both small and large scale deformation angles is still awaited.

In this paper, an 8-element singly curved conformal antenna for beamforming using eigenbeam analysis is designed and investigated. The array steering matrix is formulated which contains the phase of incident plane wave at each of the antenna elements on a conformal singly curved surface. Then an estimate of the correlation matrix is built from the signal and noise samples. The eigen decomposition of the correlation matrix gives the complex array weights. Finally, expression for array factor is developed by incorporating the effects of individual antenna element patterns and deformation angles of conformal surface. The complex array weights computed are used in the developed array factor expression to generate the signal eigenbeams and eigenvalues for different amount of surface deformations and various angles of incident signal(s). Conformal antenna array geometry, its eigenbeam analysis, effects of surface deformation, experimental validation, and effects of eigenvalues parameters are explained in the following sections.

## 2. GEOMETRY OF SINGLY CURVED CONFORMAL ANTENNA ARRAY

Geometrical layout of the 8-element patch antenna array on the exterior of a non-conducting corner structure (singly curved conformal surface) is shown in Figure 1. Each of the two faces of the anhedral corner type structure supports four patch antenna elements. The deformation angle of the conformal structure is denoted by $\Upsilon_d$, which for example may represent an anhedral angle of an aircraft wings. The intentional and unintentional flexing of wings will cause $\Upsilon_d$ to change in real time, and thus, it is the representation of static and/or dynamic environmental conditions (due to severe weather conditions, loads, flexing with purpose, etc). The value of $\Upsilon_d = 0$ corresponds to antenna elements lying along $x$-axis (linear array). The increasing values of $\Upsilon_d$ represents more bending and more surface deformation.

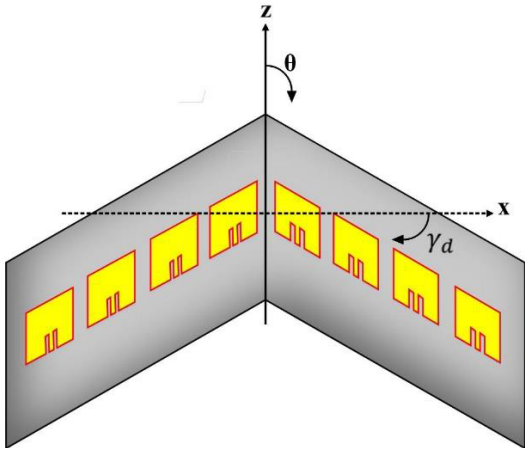


**Figure 1.** Geometry of singly curved conformal array of eight microstrip patch antennas mounted on an anhedral corner structure.

## 3. EIGENBEAM ANALYSIS

Consider $M$ signal wavefronts incident at different angles on the conformal antenna array as shown in Figure 2. For clarity, the $m$th signal wavefront with propagation vector $\hat{k}$ is drawn at the centre of coordinate system as shown in Figure 3. For $0 < \theta < \Upsilon_d$, the phase of signal wavefront incident at patch antenna elements on right face of anhedral corner structure is represented by $e^{jk\left(\frac{2n+1}{2}\right)d\sin(\Upsilon_d-\theta_m)}$, and its phase is represented by $e^{jk\left(\frac{2n+1}{2}\right)d\sin(\Upsilon_d+\theta_m)}$ at patch antenna elements on the left face of corner structure. The signs of arguments are changed for observation angle $\theta < 0$. $n = 0, 1, ..., N/2$,

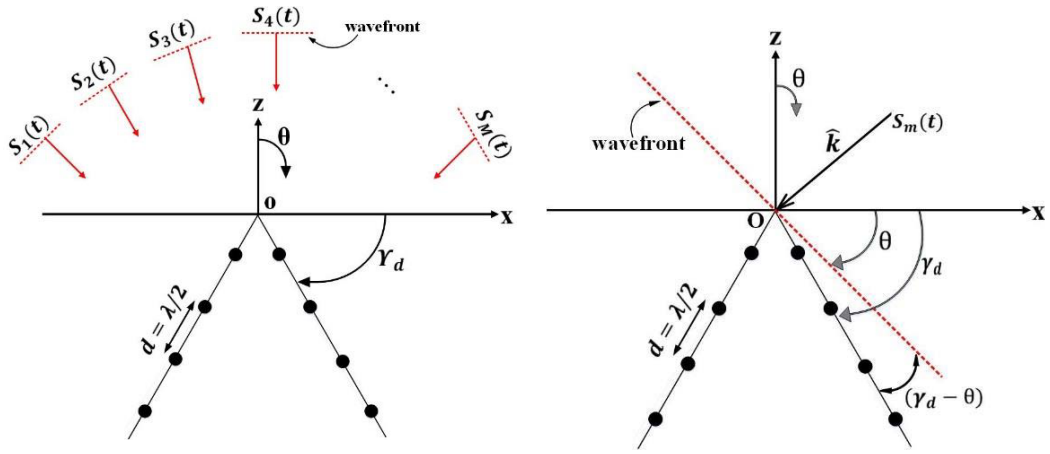


**Figure 2.** (a) Incident signals on 8-element anhedral conformal structure with deformation angle of $\Upsilon_d$ and (b) illustration of the 8-element conformal antenna on an anhedral corner structure with reference wavefront at angle $\theta$.

$m = 0, 1, ..., M$, where $N$ is the total number of antenna elements and $M$ the number of incident signals. Next, the array steering matrix is formed with phases of incident wavefronts on each antenna element of the conformal array as given below [3]:

$$A_s = \begin{bmatrix} e^{jk\left(\frac{2n+1}{2}\right)d\sin(\Upsilon_d \pm \theta_1)} & e^{jk\left(\frac{2n+1}{2}\right)d\sin(\Upsilon_d \pm \theta_2)} & \dots & e^{jk\left(\frac{2n+1}{2}\right)d\sin(\Upsilon_d \pm \theta_M)} \\ e^{jk\left(\frac{2n+1}{2}\right)d\sin(\Upsilon_d \pm \theta_1)} & e^{jk\left(\frac{2n+1}{2}\right)d\sin(\Upsilon_d \pm \theta_2)} & \dots & e^{jk\left(\frac{2n+1}{2}\right)d\sin(\Upsilon_d \pm \theta_M)} \\ \vdots & \vdots & \vdots & \vdots \\ e^{jk\left(\frac{2n+1}{2}\right)d\sin(\Upsilon_d \pm \theta_1)} & e^{jk\left(\frac{2n+1}{2}\right)d\sin(\Upsilon_d \pm \theta_2)} & \dots & e^{jk\left(\frac{2n+1}{2}\right)d\sin(\Upsilon_d \pm \theta_M)} \end{bmatrix} \tag{1}$$

The correlation matrix composed from the incident signal and noise samples at $K$ observation time intervals is given by [3]:

$$R = R_s + R_n \tag{2}$$

where

$$R_s = \frac{1}{K}\sum_{i=1}^{K} X_s(i) X_s^*(i) \tag{3}$$

is the signal correlation matrix with

$$X_s = A_s s(t), \tag{4}$$

$$s(t) = [s_1(t) \;\; s_2(t) \;\; \dots \;\; s_M(t)]^T, \tag{5}$$

$s(t)$ is the signal amplitude vector of the plane wave incident on the conformal array in Figure 2 at $\theta_m$. $T$ represents the transpose, and $*$ represents the complex conjugate transpose of the matrices.

The expression,

$$R_n = \frac{1}{K}\sum_{i=1}^{K} N(i) N^*(i) \tag{6}$$

is the noise correlation matrix. Assuming the noise to be uncorrelated from antenna element to element, the off-diagonal values of the noise correlation matrix in Eq. (6) are zero when $K$ is taken large enough, and the diagonal elements are the noise standard deviation $\sigma_n$, that is

$$R_n = \begin{bmatrix} \sigma_n & 0 & 0 \\ 0 & \ddots & 0 \\ 0 & 0 & \sigma_n \end{bmatrix} \tag{7}$$

Next, the eigen decomposition of the correlation matrix in Eq. (2) can be written as

$$R = VDV^{-1} = V \begin{bmatrix} \lambda_1 & 0 & ... & 0 \\ 0 & \lambda_2 & \ddots & \vdots \\ \vdots & \ddots & \ddots & 0 \\ 0 & \cdots & 0 & \lambda_N \end{bmatrix} V^{-1} \tag{8}$$

where $V$ is a matrix whose columns are eigenvectors, and $\lambda_n$ is an eigenvalue associated with the eigenvector.

The desired signals incident on the conformal array have the largest eigenvalues, while the noise signals have the eigenvalues equal to $\sigma_n$. The noise eigenvalues are independent of angle, while the signal eigenvalues are a function of signal direction and signal amplitude. The eigenvalues are dependent on signal and noise power values. The signal eigenvectors are the array weights to generate peak lobes in the directions of the desired signals, and noise eigenvectors are the array weights to generate nulls in the directions of the signals. If $M$ signals of interest are incident on an $N$ elements conformal antenna array ($N > M$) in Figure 2, then $M$ signal eigenvalues and $N - M$ noise eigenvalues are produced. The amount of conformal surface deformation and antenna element patterns on the conformal surface affect the eigenvalues and eigenvectors of the correlation matrix, as will be demonstrated in the next sections.

### 3.1. Eigenbeam Array Pattern for Conformal Antenna Array

The array patterns corresponding to eigenvector weights are called eigenbeams. A conformal array with positions $(x_n, z_n)$ of antenna elements lying on a curved surface in Figure 2 has an array pattern (AP) given by [2]:

$$AP_m(\theta) = \sum_{n=-\frac{N}{2}}^{-1} e_l V[:,m]\, e^{jk[x_n \sin\theta + z_n \cos\theta]} + \sum_{n=1}^{\frac{N}{2}} e_r V[:,m]\, e^{jk[x_n \sin\theta + z_n \cos\theta]} \tag{9}$$

$(x_n, z_n) = \left(\left(\frac{2n\pm1}{2} d\cos\Upsilon_d\right), \left(\frac{2n\pm1}{2} d\sin\Upsilon_d\right)\right)$ is the location of the $n$th antenna element on the conformal surface in Figure 2. The columns of matrix $V$ computed from Eq. (8) are the eigenvector array weights, and $e_l = \cos(\theta + \Upsilon_d)$, $e_r = \cos(\theta - \Upsilon_d)$ are the antenna elements patterns on left and right faces of the conformal surface. Equation (9) shows that eigenbeam array pattern is a complex function of various factors, including individual antenna element patterns on the conformal surface, complex eigenvector coefficients, and the amount of severity of surface deformations.

## 4. SIMULATION RESULTS

To validate Equations (8) and (9) for single and multiple beamformings, consider the following two cases of signal wavefronts incident at different angles on the conformal antenna array as shown in Figure 3: case (a): 1 V/m plane wavefront incident at 25° angle, and case (b): 1 V/m plane wavefront incident at −20° and 1 V/m plane wavefront incident at 30°.

Assume $\Upsilon_d = 30°$ and $\sigma_n = 0.01$. The eigenvectors and eigenvalues for the two cases are computed using Equations (1)–(8) and are displayed in Table 1. For case (a), the first seven eigenvalues are equal to $\sigma_n$, while the last one, corresponding to the desired signal, is much higher. For case (b), the first six eigenvalues are equal to $\sigma_n$, while the last two corresponding to the desired signals are much higher. As shown in Figure 3, for case (a), the signal eigenbeam associated with $V_8$ has peak at 25°, and for case (b), the signal eigenbeams associated with $V_7$ and $V_8$ have peaks at −20° and 30°. These results indicate that the expressions developed using Eqs. (1) to (9) for the conformal antenna array in Figure 3 can be used to derive complex array weights to generate the peak beam(s) towards the desired signal of interest(s). Similarly, it was observed that desired array weights can be computed for other angles of incidence and for other angles of surface deformation $\Upsilon_d$. Therefore, the expressions developed using Eqs. (1) to (9) show generalization for any angle of incidence and for any angle of surface deformation of conformal singly curved antenna array. In next sections, the effects of eigenvalues on angular separation distance between incident signals and on signal strengths for surface deformation $\Upsilon_d$ are investigated.

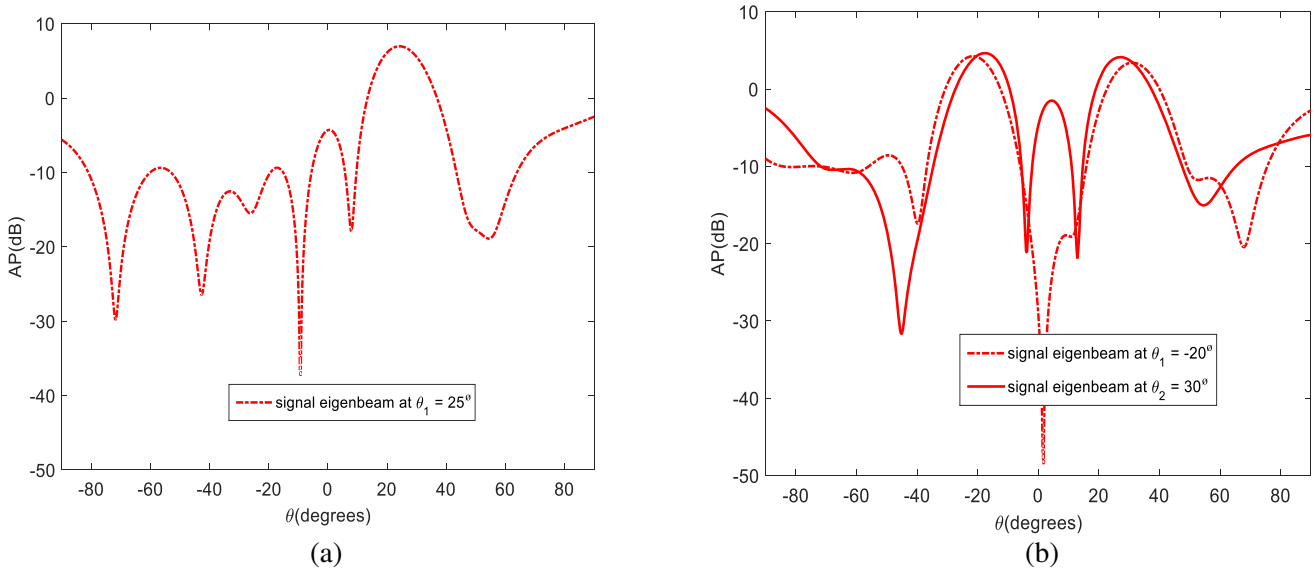


**Figure 3.** Plot of signal eigenbeams for case (a), and case (b) with $\Upsilon_d = 30°$.

**Table 1.** Eigenbeam analysis of the correlation matrix in Eq. (8) for case (a) and case (b).

| Signal eigenvectors | | | | | |
|---|---|---|---|---|---|
| Case (a) | | Case (b) | | | |
| $V_8$ | | $V_7$ | | $V_8$ | |
| Amplitudes (dB) | Phases (degrees) | Amplitudes (dB) | Phases (degrees) | Amplitudes (dB) | Phases (degrees) |
| −9.0304 | 101.1648 | −9.1237 | 266.1222 | −8.9209 | 86.2942 |
| −9.0323 | 313.7056 | −15.6589 | 352.7028 | −6.6567 | 352.6781 |
| -9.0310 | 166.2628 | -5.9705 | 259.0295 | -22.6505 | 258.8091 |
| −9.0317 | 18.8167 | −10.3851 | 165.4119 | −8.0428 | 345.5822 |
| −9.0317 | 312.9320 | −12.1167 | 333.2176 | −7.3593 | 333.2081 |
| −9.0311 | 328.6083 | −5.9563 | 42.0860 | −23.0157 | 222.4851 |
| −9.0303 | 344.3109 | −18.8550 | 110.8730 | −6.3861 | 291.1218 |
| −9.0287 | 0 | −7.4985 | 0 | −11.2498 | 0 |
| Signal eigenvalues | | | | | |
| Case (a): [0.0074 0.0080 0.0087 0.0095 0.0096 0.0105 0.0119 8.0096] | | | | | |
| Case (b): [0.0086 0.0088 0.0103 0.0111 0.0117 0.0128 7.5214 8.5132] | | | | | |

### 4.1. Effects of Surface Deformation on Eigenbeam

The eigenbeam for case (a) in Table 1 is investigated for different angles of surface deformation as shown in Figure 4. In Chapter 5 of [3], angles from $\Upsilon_d = 0°$ to $\Upsilon_d = 20°$ are defined as small angles, and those above $\Upsilon_d = 20°$ are considered as large flex angles for wedge-shaped conformal surface. Keeping this in mind, the effects from $\Upsilon_d = 0°$ (flat array) to $\Upsilon_d = 45°$ has been investigated in this research work and is demonstrated in Figure 4. The middle bend angle case of $\Upsilon_d = 30°$ has been validated in measurements. The case of $\Upsilon_d = 0°$ is taken as a reference and represents the flat antenna array. As the angle of deformation increases from $\Upsilon_d = 0°$ to $\Upsilon_d = 45°$, the half-power beamwidth (HPBW) of main beam increases approximately by 5.5°; first-null beamwidth (FNBW) increases by approximately

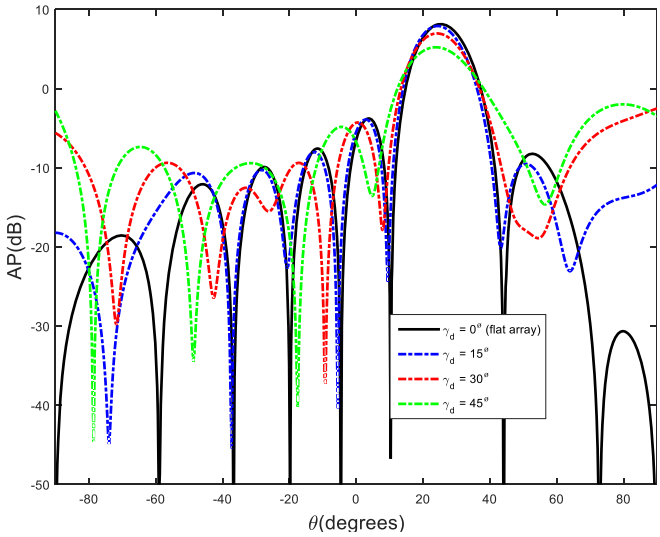


**Figure 4.** Plot of array patterns using (9) for different surface deformations.

18°; and peak gain of main beam decreases by about 2.8 dB. Similar behaviour was observed for case (b) of signal eigenbeams.

### 4.2. Eigenvalues vs Angular Separation Distance

To investigate the effects of eigenvalues vs angular separation distance between incident signals on the 8-element conformal antenna array in Figure 2 with $\Upsilon_d = 30°$, we consider two equally weighted signals incident on the array ($\sigma_n = 0.01$). The first signal is incident at $\theta_1 = 0°$, and the other signal is incident at $-50° \leq \theta_2 \leq 50°$. The eigenvalues plot in Figure 5(a) shows that $\lambda_1$ of the first signal begins to increase, and $\lambda_2$ decreases as signal $s_2$ enters the main beam. When both signals are incident at $\theta = 0°$, $\lambda_1$ approximately doubles, and $\lambda_2$ is approximately zero and indistinguishable from the noise eigenvalues. The eigenbeam plot for this scenario is shown in Figure 5(b). Similarly, behaviour was observed for other deformation angles $\Upsilon_d$.

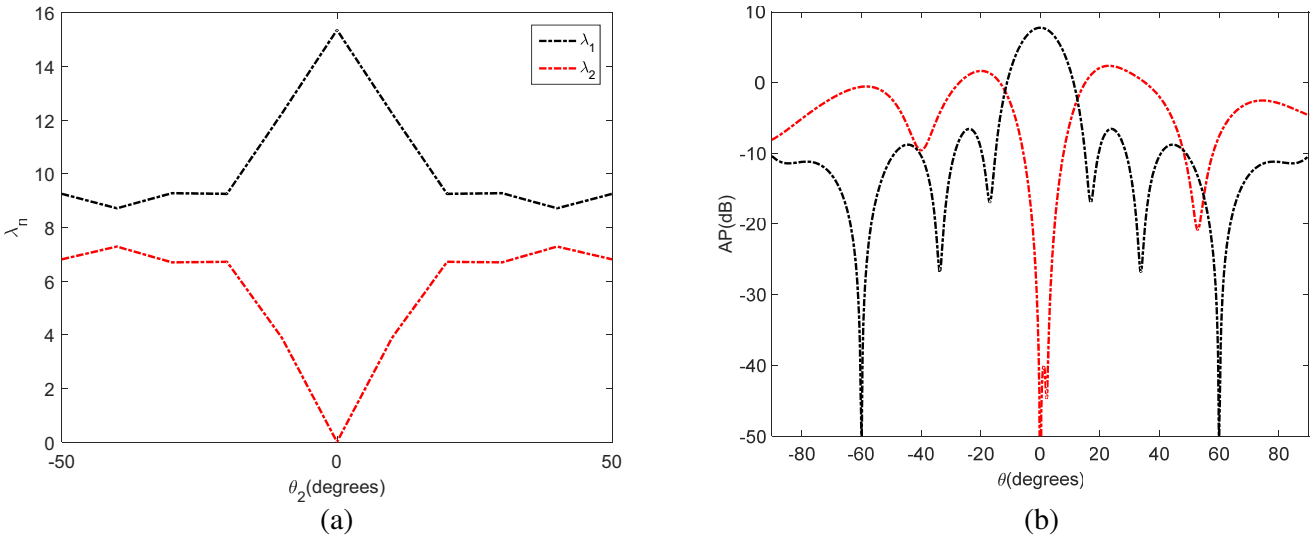


**Figure 5.** Plot of (a) eigenvalues versus angular separation distance, and (b) eigenbeams for incident signals at angles $\theta_1 = \theta_2 = 0°$ (angular separation distance = 0).

### 4.3. Eigenvalues Versus Signal Strength Ratio

To investigate the effects of signal strengths, consider two signals incident on the array in Figure 2 with amplitude of the first signal $s_1 = 1$ incident at $\theta_1 = 0°$ and $0 \leq s_2 \leq 2s_1$ incident at $\theta_2 = 40°$. Assume $\sigma_n = 0.01$ and $\Upsilon_d = 30°$. Figure 6 shows the eigenvalues graphed as a function of $s_2/s_1$. When $s_2 = 0$, $\lambda_1 = 8$ and $\lambda_2 = \sigma_n$. When $s_2$ is increased until it equals $s_1$, $\lambda_1$ stays approximately constant, while $\lambda_2$ increases. When $s_2 > s_1$, $\lambda_2$ stays approximately constant while $\lambda_1$ increases. The largest eigenvalue always corresponds to the most powerful signal. Similar behaviour was observed for other angles of surface deformation.

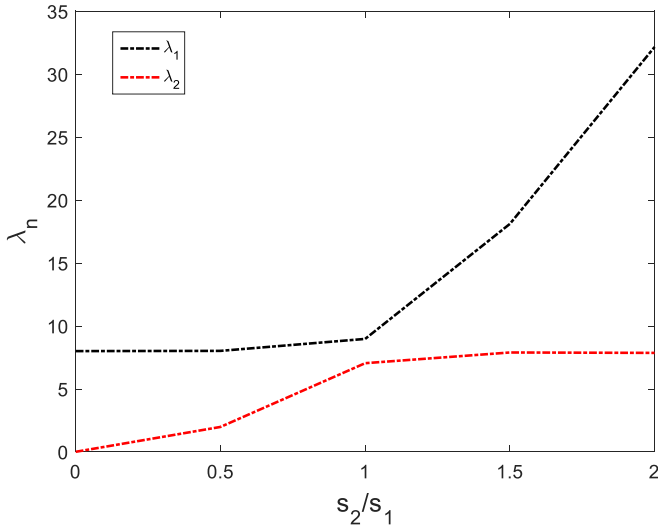


**Figure 6.** Plot of eigenvalues versus signal strength ratio between two signals incident on the 8-element singly curved conformal antenna array with $\Upsilon_d = 30°$.

**Discussion**: At this point, it would be interesting to compare the proposed beamforming technique with relevant work in the literature. In [8], genetic algorithm is employed to place a deep null in the array pattern. In each iteration of the adaptive algorithm, new phase and amplitude settings are required to minimize the output power of the array to obtain the desired null location, which is not feasible in real-time applications for conformal surfaces that change shape with time. In contrast, the proposed technique computes the complex weights (amplitudes and phases) by correlating the desired signal with interferers, which is done one time and then can be stored in a look-up table, thereby greatly reducing the complexity. In [10–13], main beam scanning is achieved using least-squares solution. The drawback of the least-squares solution is probability of getting small singular values, which can dramatically deteriorate the main beam and change the nulls location of the radiation pattern. Although the possible solution may discard all singular values below a certain threshold, discarding too many singular values will result in a deteriorated radiation pattern. This problem is solved in the proposed solution by computing the response of desired signal weights at nulls location and simply subtracting them to calculate the final array weights. In [18, 19], optimization algorithms are used to calculate the excitation phases for the generation of single and multiple main beams; therefore, only single degree of freedom (phase) is available. The proposed solution computes both amplitudes and phases to give better control over nulls location and their depth.

## 5. MEASUREMENT RESULTS

For measurement validation of the eigenbeam patterns generated using Eqs. (8) and (9) for conformal antennas placed on anhedral corner type structure, two cases (a) and (b) as discussed in Section 'simulation results' will be considered. An 8-element microstrip patch antenna array with inter-element spacing of $0.5\lambda_0$ and working at 2.45 GHz was placed on the non-conducting anhedral corner structure

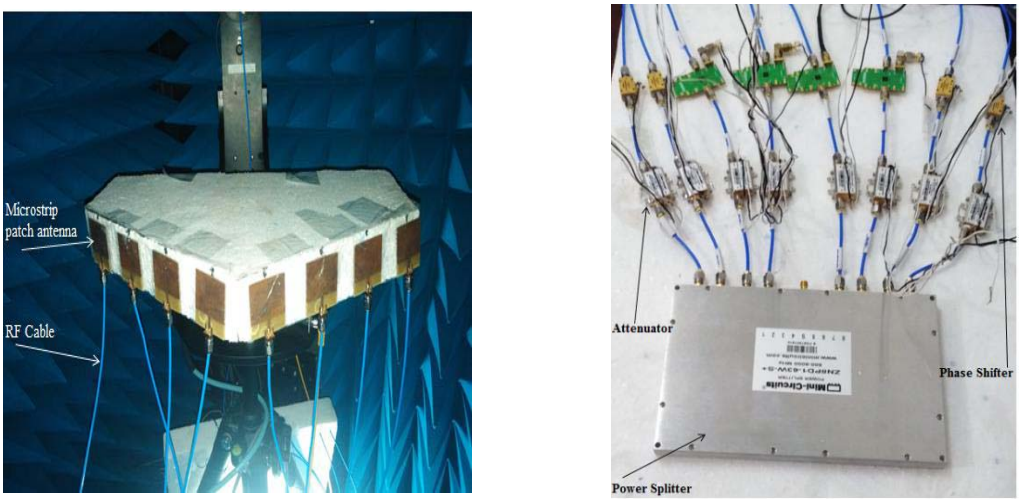


(a) (b)

**Figure 7.** Photograph of (a) 8-element singly curved conformal antenna array with $\Upsilon_d = 30^\circ$ in an anechoic chamber, (b) feed network.

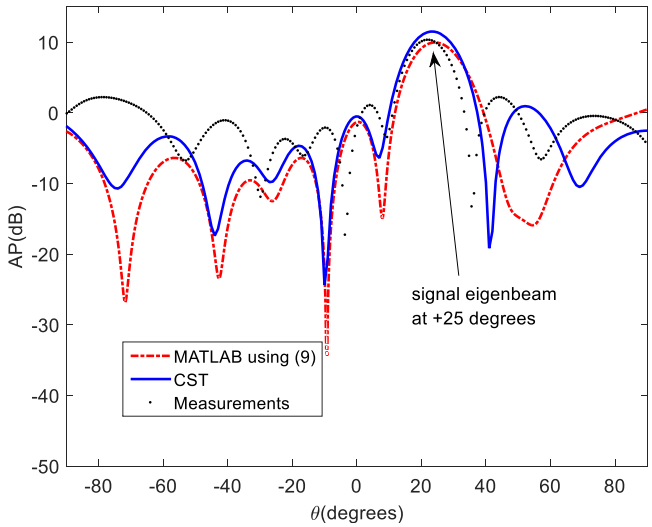


**Figure 8.** Plot of signal eigenbeam on the 8-element singly curved conformal antenna array with $\Upsilon_d = 30^\circ$ for case (a) in Table 1 using signal eigenvector $V_8$.

with $\Upsilon_d = 30^\circ$ as shown in Figure 7(a). Each patch antenna element was separately excited with complex signal eigenvectors computed using Eq. (8) through commercial off the shelf microwave components: phase shifter and attenuator through power splitter and RF cables as shown in Figure 7(b). The measured eigenbeam array patterns for the two cases (a) and (b) are shown in Figures 8 and 9, respectively. For comparison, CST and MATLAB results are also given in Figures 8 and 9. As shown in Figure 8, for case (a), the main beam of array pattern corresponding to signal eigenvector $V_8$ in Table 1 is directed towards the desired incident signal of interest at $\theta_1 = 25^\circ$. Similarly as shown in Figure 9, for case (b), two main beams of array pattern corresponding to signal eigenvectors $V_7$ and $V_8$ in Table 1 are directed towards the incident signals of interest at $\theta_1 = -20^\circ$ and $\theta_2 = 30^\circ$. For both cases, the MATLAB, CST, and measurement results are in good agreement at desired incident angles $(25^\circ, -20^\circ, 30^\circ)$ of signal eigenbeams plot. This demonstrates the validity of the expressions developed in Eqs. (8) and (9) to generate the eigenbeams using conformal antenna array.

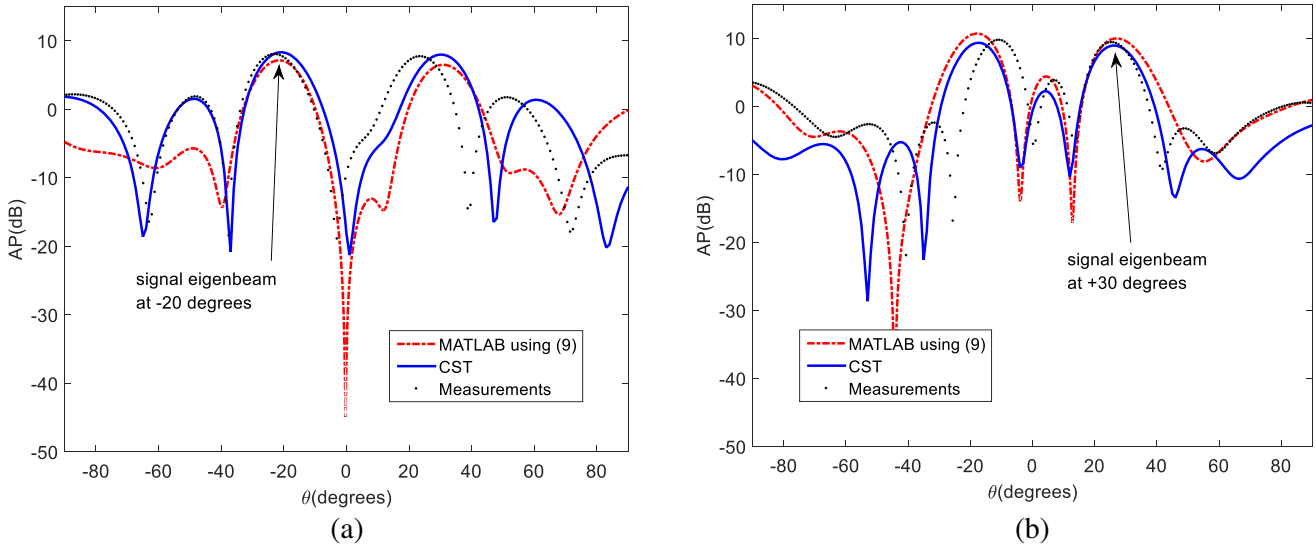


**Figure 9.** Plot of signal eigenbeam on the 8-element singly curved conformal antenna array with $\Upsilon_d = 30°$ for case (b) in Table 1 using signal eigenvector $V_7$. (b). Plot of signal eigenbeam on the 8-element singly curved conformal antenna array with $\Upsilon_d = 30°$ for case (b) in Table 1 using signal eigenvector $V_8$.

## 6. CONCLUSION

Eigenbeam analysis to generate the single/multiple main beam(s) towards the desired signal(s) incident on the conformal antenna array for different angles of surface deformation is developed. The analysis is validated through analytical, simulated, and measured results which shows that the presented technique can be used for both small and large scale deformation angles. Furthermore, the effects of eigenvalues on angular separation distance between incident signals and on signal strengths are discussed. It is shown that when angular resolution between two incident signals becomes small, they become indistinguishable, and eigenvalue approaches $\sigma_{\text{noise}}$. The largest eigenvalue always corresponds to the most powerful signal. The gain of main beam drops, and beamwidth widens for increasing amount of surface deformations.

## ACKNOWLEDGMENT

This work is supported by Ignite (National Technology Fund), Ministry of IT & Telecom, Government of Pakistan via project No. ICTRDF/TR&D/2015/04.

## REFERENCES

1. Josefsson, L. and P. Persson, *Conformal Array Antenna Theory and Design*, Wiley-IEEE Press, USA, 2006, doi: 10.1002/047178012X.
2. Hansen, R. C., *Phased Array Antennas*, 2nd edition, John Wiley and Sons, New York, 2010.
3. Haupt, R. L., *Antenna Arrays, A Computational Approach*, Wiley-IEEE Press, USA, 2010.
4. Salonen, P., Y. Rahmat-Samii, M. Schaffrath, and M. Kivikoski, "Effect of textile materials on wearable antenna performance: A case study of GPS antennas," *IEEE International Symposium on Antennas and Propagation*, Monterey, USA, June 2004.
5. Kennedy, T. F., P. W. Fink, A. W. Chu, N. J. Champagne, G. Y. Lin, and M. A. Khayat, "Body-worn E-textile antennas: The good, the low-mass, the conformal," *IEEE Transactions on Antennas and Propagation*, Vol. 57, 910–918, 2009, doi: 10.1109/TAP.2009.2014602.

6. Kuang, Y., L. Yao, S.-H. Yu, S. Tan, X.-J. Fan, and Y.-P. Qiut, "Design and electromagnetic properties of a conformal ultra wideband antenna integrated in three-dimensional woven fabrics," *Polymers MDPI*, Vol. 10, 1–10, 2018, doi: 10.3390/polym10080861.
7. Semkin, V., A. Bisognin, M. Kyrö, V.-M. Kolmonen, C. Luxey, F. Ferrero, F. Devillers, and A. V. Räisänen, "Conformal antenna array for millimeter-wave communications: Performance evaluation," *International Journal of Microwave and Wireless Technologies*, Vol. 9, 241–247, 2017, doi: 10.1017/S1759078715001282.
8. Pourya, A. and S. R. Seydnejad, "Broadband adaptive beamforming of conformal arrays for wireless communications based on generalized sidelobe canceller," *Wireless Personal Communications*, Vol. 96, 1131–1143, 2017, doi: 10.1007/s11277-017-4228-x.
9. Schippers, H., P. Knott, T. Deloues, P. Lacomme, and M. R. Scherbarth, "Vibrating antennas and compensation techniques research in NATO/RTO/SET 087/RTG 50," *IEEE Aerospace Conference*, Big Sky, USA, 2004.
10. Loecker, C., P. Knott, R. Sekora, and S. Algermissen, "Antenna design for a conformal antenna array demonstrator," *6th European Conference on Antennas and Propagation (EuCAP)*, Prague, Czech Republic, March 2012.
11. Knott, P., H. Schippers, et al., "Performances of conformal and planar arrays," *NATO Symposium on Smart Antennas, Proceedings*, P13.1–P13.10, 2003.
12. Sharawi, M. S., D. N. Aloi, and O. A. Rawashdeh, "Design and implementation of embedded printed antenna arrays in small UAV wing structures," *IEEE Transactions on Antennas and Propagation*, Vol. 58, 2531–2538, 2010, doi: 10.1109/TAP.2010.2050440.
13. Anagnostou, D. and M. Iskander, "Adaptive flexible antenna array system for deformable wing surfaces," *IEEE Aerospace Conference*, Big Sky, USA, March 2015.
14. Braaten, B. D., M. A. Aziz, S. Roy, S. Nariyal, Irfanullah, N. F. Chamberlain, M. T. Reich, and D. E. Anagnostou, "A self-adapting flexible (SELFLEX) antenna array for changing conformal surface applications," *IEEE Transactions on Antennas and Propagation*, Vol. 61, 655–665, 2013, doi: 10.1109/TAP.2012.2226227.
15. Irfanullah, S. Khattak, and B. D. Braaten, "Improvement of the broadside radiation pattern of a conformal antenna array using amplitude tapering," *Applied Computational Electromagnetic Society (ACES) Journal*, Vol. 32, 511–516, 2017.
16. Irfanullah, S. Khattak, and B. D. Braaten, "Broadside pattern correction techniques for conformal antenna arrays," *Advances in Array Optimization*, E. Aksoy, Chapter 5, IntechOpen, London, UK, 2020.
17. Knott, P., "Antenna design and beamforming for a conformal antenna array demonstrator," *IEEE Aerospace Conference*, Big Sky, USA, July 2006.
18. Schippers, H., J. Verpoorte, P. Jorna, A. Hulzinga, A. Meijerink, C. Roeloffzen, R. G. Heideman, A. Leinse, and M. Wintels, "Conformal phased array with beam forming for airborne satellite communication," *2008 International ITG Workshop on Smart Antennas*, Vienna, Austria, July 2008.
19. Sun, D., R. Shen, and X. Yan, "A broadband conformal phased array antenna on spherical surface," *International Journal of Antennas and Propagation*, 1–5, 2014, doi: 10.1155/2014/206736.
20. Kumar, R., P. Kumar, and M. V. Kartikeyan, "Wide scanned electronically steered conformal active phased array antenna for Ku-band SATCOM," *International Journal of Microwave and Wireless Technologies*, Vol. 11, 376–381, 2019, doi: 10.1017/S1759078718001599.
21. Bouwmeester, W., "Conformal phased array for disturb," MS Thesis, Delft University of Technology, 2020.